

1
2 **EFFECT OF SULFUR ON SIDEROPHILE ELEMENT PARTITIONING**
3 **BETWEEN OLIVINE AND MARTIAN MANTLE PRIMARY MELT**

4
5 Revision 1.1

6
7 Tomohiro Usui^{1,2,5}, Kevin Righter^{2,5}, Charles K. Shearer^{3,4}, and John H. Jones⁴,

8
9 ¹ Institute of Space and Astronautical Sciences, Japan Aerospace Exploration Agency,
10 Kanagawa, 252-5210, Japan

11
12 ² NASA Johnson Space Center, Mailcode XI2, 2101 NASA Pkwy, Houston, TX 77058

13
14 ³ Institute of Meteoritics, University of New Mexico, Albuquerque, NM 87131

15
16 ⁴ Lunar and Planetary Institute, 3600 Bay Area Blvd., Houston, TX 77058

17
18 ⁵ These authors contributed equally to this work

19
20

21 *Abstract* - Ni and Co variations in primary martian magmas exhibit anomalous incompatible
22 behavior, which has remained an unexplained conundrum. Because martian magmas are S-rich,
23 and some trace metals have reported enhanced solubility in S-bearing magmas, we have carried
24 out a series of experiments to evaluate the effect of high-S melts on the olivine/melt partitioning
25 of Ni, Co, Mn, V, and Cr. Near-liquidus experiments on a synthetic primary martian mantle melt
26 (Yamato-980459 [Y98]) were completed in a piston cylinder apparatus at 0.75 GPa. Previous
27 studies in S-free systems illustrate that the partition coefficients for these elements are dependent
28 chiefly on $D(\text{Mg})_{\text{ol/melt}}$ (the partition coefficient defined as wt% Mg in olivine / wt% Mg in melt),
29 a proxy for temperature, and were used to calibrate a predictive expression that includes the
30 effects of temperature [i.e., $D(\text{Mg})_{\text{ol/melt}}$], melt composition, and oxygen fugacity. These
31 predictive expressions are then used to isolate any effect in $D(\text{M})_{\text{olivine/melt}}$ due to dissolved
32 sulfur. The results show that S might have a small effect for Co, but not enough to change Co
33 partitioning from compatible to incompatible in our experiments. Addition of a sulfur term to
34 the $D(\text{Co})_{\text{olivine/melt}}$ predictive expressions shows that nearly 8000 ppm of sulfur would be required in the
35 melt (at liquidus temperature of Y98) for $D(\text{Co})_{\text{olivine/melt}}$ to become <1 . These S contents are 2 times
36 higher than those of a sulfide saturated melt at the (P,T) conditions of a martian mantle source
37 region. Therefore, the anomalous incompatible behavior observed in these primary magma
38 suites must be due to another mechanism. High temperature, oxygen fugacity, and diffusion are
39 not viable mechanisms, but magma mixing, assimilation, or kinetic crystallization effects remain
40 possibilities.

41

42

43 Keywords: shergottite; olivine; transition metals; sulfur; basaltic magma

44

45

46 **Introduction**

47 First-row transition elements (FRTE, including Mn, Ni, Co, Fe, V, and Cr) are useful
48 indicators of primary planetary mantle melts (Sato, 1976; Wänke and Dreibus, 1986) and the
49 source mineralogy of mantle melts (Sobolev et al., 2007), and their ratios can be used to infer
50 source heterogeneities in mantle-derived melts (e.g. Fe/Mn; Humayun et al., 2004; LeRoux et al.,
51 2011). Since olivine is a common early-crystallizing phase in basaltic magmas that have
52 produced planetary and asteroidal crusts, a number of experimental studies have investigated
53 elemental partitioning between olivine and silicate melt (e.g., Toplis, 2005; Libourel, 1999;
54 Jones, 1995). In particular, olivine/melt partition coefficients of Ni and Co ($D(\text{Ni})$ and
55 $D(\text{Co})_{\text{ol/melt}}$) have been intensively studied because these elements are preferentially partitioned
56 into olivine and thus provide a uniquely useful insight into the basalt petrogenesis (e.g.,
57 Takahashi, 1978; Beattie et al., 1991; Longhi et al., 2010). Ni and Cr have both been used as
58 indicators of primary melts of planetary mantles (e.g., Sato, 1977; Wänke and Dreibus, 1986;
59 Sobolev et al., 2007). Vanadium partitioning between olivine and melt is sensitive to changes of
60 oxygen fugacity and has been used as an oxybarometer (Shearer et al., 2006; Mallmann and
61 O'Neill, 2013; Lee et al., 2003; Canil and Fedortchouk, 2001; Nakada et al. 2020). Chromium
62 partitioning between olivine and melt is also dependent upon oxygen fugacity since Cr^{2+} is stable
63 in melts at low $f\text{O}_2$ (e.g., Hanson and Jones, 1998). Finally, Mn partitioning differences
64 between peridotite and pyroxenite can be used to place constraints on sources of mantle melts
65 (LeRoux et al., 2011; Sobolev et al., 2007). Fe/Mn ratios in meteorites are used to trace the
66 origins of various meteorite groups due to the variable volatility of Mn in the solar system (e.g.,
67 Papike, 1998; Goodrich and Delaney, 2000; Karner et al., 2003), but a comprehensive
68 interpretation of this ratio must include an understanding of differences in olivine melt

69 partitioning for Fe and Mn. Overall, the FRTE are very useful in delineating source
70 characteristics and origin of planetary basalts.

71 Extensive studies of olivine/melt partitioning of FRTE have demonstrated the role of
72 pressure, temperature, oxygen fugacity, and melt composition in controlling the magnitude of D
73 (olivine/melt) (e.g., Takahashi, 1978; Beattie et al., 1991; Matzen et al., 2013; Longhi et al.,
74 2010; Elardo et al., 2011; Hanson and Jones, 1998; Mallmann and O'Neill, 2013; LeRoux et al.,
75 2011; Filiberto et al., 2009). Despite the many studies carried out on the partitioning behavior
76 of Ni and Co, basic chemical trends in terrestrial and planetary samples remain unexplained. For
77 example, Co exhibits incompatible behavior in olivines from Martian meteorites and lunar
78 basalts, while Ni exhibits compatible behavior (**Figure 1**; Papike et al. 2009; Usui et al., 2008;
79 Karner et al., 2003). High temperatures (~ 2000 °C) might be the cause of the opposite behavior
80 of Ni and Co as shown by Longhi et al. (2010) and Elardo et al. (2011) for lunar magma ocean
81 conditions, but these temperatures are much higher than liquidus temperatures of the olivine-
82 phyric shergottites, near 1500 °C at 0.5 GPa (e.g., Rapp et al., 2013) and therefore cannot be the
83 cause of the incompatible behavior. Similarly, Ni and Co exhibit de-coupled behavior in
84 terrestrial peridotite and pyroxenite, compared to their expected compatible behavior (Sobolev et
85 al., 2007; Herzberg et al., 2016).

86 A distinctive aspect of martian magmas and shergottites that might provide an
87 explanation for compatible Ni and incompatible Co is the high S contents of primitive shergottite
88 liquids (up to 2700 ppm; Franz et al., 2014). Sulfur is known to enhance the solubility of some
89 trace metals in terrestrial magmas. For example, chemical analyses of S-rich Mid-Ocean Ridge
90 Basalt (MORB) samples (i.e. un-degassed with respect to sulfur) suggest that S dissolved in
91 silicate melts can reduce $D(\text{Ni})_{\text{ol/melt}}$ up to 50 % compared to S-free experimental systems (Li et

92 al., 2003). MORB glasses typically contain ~ 1000 ppm S at 8% MgO (e.g. Le Voyer, et al.,
93 2019), and even at those concentration levels, S has a discernable effect on D(Ni) olivine/melt.
94 Martian basaltic melts are known to contain even higher S contents (up to 2700 ppm; Dreibus et
95 al., 1982, 2000; Zipfel et al., 2000; Shirai and Ebihara, 2004; Franz et al., 2014). The high S
96 contents of shergottites in general as well as the high solubility of S in primitive shergottite melts
97 (up to 4000 ppm; Righter et al., 2009) implies that S might be responsible for significantly
98 influencing the Ni, Co, and other FRTE partitioning in shergottite olivines. Although Mn, V,
99 and Cr all exhibit incompatibility in olivine for martian magmatic conditions (e.g., Karner et al.,
100 2007; Righter et al., 2006; Hanson and Jones, 1998), the extent of their incompatibility (e.g. Mn
101 in Herd et al., 2009) must be explored in S-bearing systems. Existing experimental data are not
102 ideal for evaluating these effects for martian melt compositions at martian mantle and magmatic
103 conditions. There are some studies that utilized S-bearing melts, but do not include martian
104 compositions (e.g. Tuff et al., 2010), or have been carried out at low PT conditions that are not
105 directly relevant to martian melt generation (e.g., Gaetani and Grove, 1997). Thus, the relevant
106 set of P-T-fO₂ conditions and melt compositions have not yet been explored together in one
107 study, and utilizing literature data would require extrapolation of one or more variables.

108 To explore the possible effects of S on the olivine/melt partitioning behavior of Ni, Co,
109 Mn, V, and Cr, we have conducted experiments to examine partitioning between olivine and
110 Martian primary mantle melt at Martian magmatic conditions (give P, T, fO₂) and variable and
111 high S contents (up to 3000 ppm). Conditions of Martian magma genesis have been explored by
112 several studies, and multiple saturation is thought to occur from 0.8 to 2 GPa and 1450 to 1575
113 °C (e.g., Rapp et al., 2013; Collinet et al., 2015; Filiberto et al., 2010; Gross et al., 2011). Given
114 the known negative pressure dependence of sulfide saturation and S solubility in melts (Righter

115 et al. 2009; Holzheid and Grove, 2002), we chose the low pressure end of this range to allow the
116 maximum values of S solubility - up to ~3000 ppm. In addition, oxygen fugacity was defined
117 below the FMQ (fayalite-magnetite-quartz) buffer which is an appropriate value for the Martian
118 mantle. The most primitive, unfractionated mantle melts are thought to be the olivine-phyric
119 shergottites high MgO (15-20 wt%) and relatively low Al₂O₃ (<7 wt%). Therefore we chose the
120 Yamato-980459 olivine-phyric shergottite as a starting composition for the experiments; this
121 sample has also been featured in studies of Ni, Co, and V in olivines (Usui et al., 2008; Nakada
122 et al., 2020) and thus is directly relevant to the results. The new results on this S-bearing
123 martian melt composition, obtained at conditions of martian magma genesis, are then used to
124 interpret trace metal contents in martian magmatic suites. The FRTE are very useful elements
125 utilized in determining source characteristics and origin of planetary basalts, and evaluation of
126 the role of S will make their prediction more accurate and applicable to natural systems such as
127 martian magmas.

128 **Experimental and analytical methods**

129 Y-980459 is an olivine-phyric shergottite (martian meteorite) interpreted as representing
130 a Martian primary mantle melt based on its bulk and olivine Mg#, Ni and Cr contents (Usui et
131 al., 2008; Greshake et al. 2004), is ideal for this study, and experiments employed a synthesized
132 Y-980459 composition (Shirai and Ebihara, 2004) for major and minor elements. Synthetic
133 glass of the Y-980459 composition was prepared from reagent grade oxide powders in an agate
134 mortar. This mixture was then fused into glass at fO₂ of ~FMQ buffer, and then reground into a
135 powder followed by addition of ~200 ppm V, Co and Ni. This starting composition was then
136 split into four aliquots; each of them was prepared to contain 0, 1000, 2000, and 3000 ppm S,

137 respectively, by the addition of pyrite (FeS₂) powder. The addition of minor amount of FeS₂ (up
138 to 3000 ppm) did not alter the phase relations of the run products.

139 Melting experiments were conducted using a Quickpress non-end-loaded piston-cylinder
140 apparatus at Johnson Space Center (JSC). Pressure was generated within BaCO₃ cells, and
141 calibrated on the location of the diopside-melting curve; pressures were corrected by -0.3 kbar
142 and only corrected pressures are reported [see Filiberto et al. (2008) for calibration results].
143 Experimental details of pressure, temperature and the assemblies were also presented in Righter
144 et al. (2009) and Filiberto et al. (2008). Samples were heated with graphite furnaces. A type C
145 thermocouple (W-Re) wire, with an accuracy of ±2 °C, was used to measure the temperature.
146 Samples were pressurized to the desired pressure (0.75 GPa), and then heated above the liquidus
147 temperature (1525 °C) for 0.5 hour before dropping to the target temperatures of 1450, 1475, and
148 1500 °C. The initial superheating followed by cooling to sub-liquidus temperatures is to
149 promote growth of large olivine crystals, as superheating should destroy more olivine nucleation
150 sites in the melt. Experiments were terminated by power quenching the samples, usually
151 resulting in glassy run products.

152 All major elements in olivines and glasses were analyzed with a Cameca SX100 electron
153 microprobe at NASA-JSC, using an accelerating voltage of 20 kV and sample current of 20 nA.
154 Standards included both natural (kaersutite, andradite, wollastonite, chromite, rutile, olivine,
155 rhodonite, potassium feldspar, albite) and synthetic (V metal, NiO) standard materials. Count
156 times for major elements were typically 10 s, and as long as 120 s for low concentrations of V or
157 Cr in olivines and glasses. Under the latter conditions, detection limits were approximately 100
158 ppm for V. Interference of TiK α on VK α peaks (Snetsinger et al. 1968) were avoided by
159 counting Ti on PET using integral mode, and V on LiF in differential mode. PAP ϕ - ρ -Z

160 corrections were used in data reduction (Pouchou and Pichoir, 1991). All analyses are reported in
161 **Tables 1 and 2.**

162 Ion microprobe analyses of experimental charges were conducted using a Cameca IMS 4f
163 instrument at the University of New Mexico following the approach of Shearer et al. (1990,
164 2005, 2006) The olivine analyses involved repeated cycles of peak counting on $^{51}\text{V}^+$, $^{59}\text{Co}^+$,
165 $^{60}\text{Ni}^+$, and $^{30}\text{Si}^+$. Ten cycles were used per analysis. The $^{30}\text{Si}^+$ was used as a reference species.
166 The analytical procedure included counting on a background position to monitor detection noise.
167 Background was collected on each standard and unknown at mass 18.7. Measurements at this
168 mass produced a background of 1-3 counts. Absolute concentrations of each element were
169 calculated using empirical relationships of measured peak $^{51,59,60}\text{X}^+ / ^{30}\text{Si}^+$ ratios normalized to
170 known SiO_2 content (calibration curves are $((^{51,59,60}\text{X}^+ / ^{30}\text{Si}^+) \times \text{SiO}_2)$ plotted against trace
171 elements for each standard) to element concentrations as derived from daily calibration
172 measurements of the following olivine and glass standards: KAUG, K1OPX, D1OL, PM150,
173 SC, MARJ, 610, 614, WUSTL1, and WUSTL2. Calibration curves for these elements have
174 previously been determined by Papike et al.(1999) and Shearer et al. (1996, 2006). Analyses
175 were made by bombardment of the sample with primary O^- ions accelerated through a nominal
176 potential of 10 kV. A primary ion current of 15-20 nA was focused on the sample over a spot
177 diameter of 15 μm . Sputtered secondary ions were energy filtered using a sample offset voltage
178 of -105 V, and an energy window of ± 25 V, to eliminate effectively most isobaric interferences
179 (Shimizu et al., 1978). Secondary ions are detected by an electron multiplier in pulse counting
180 mode. Peak counting times were varied to optimize precision. For olivine and glass analyses,
181 precisions of better than 3% and 5%, respectively, were achieved. All ion microprobe analyses
182 were conducted at locations analyzed previously with the electron microprobe, and the SiO_2

183 concentrations determined by EMP were used in reducing the SIMS data. Inclusion of
184 contaminating phases in the SIMS analyses was avoided by selecting optically clean olivine
185 grains and by mass imaging of major elements before and after each spot SIMS analysis.

186 **Results**

187 *Phase equilibrium*

188 Experimental charges mainly consist of olivine (Fo₈₁₋₈₄) and glass (**Figure 2**). Melt
189 fractions were determined by using Ca mass balance between the bulk composition, glass and
190 olivine, and varied from 0.85 to 0.98 in weight. Spinel is present only in two 1450 °C charges,
191 the lowest temperature of our experimental suite. No sulfide phases are observed in the charges,
192 suggesting sulfide under-saturation. Run products were sliced vertically to ensure that sulfide
193 liquids had not settled to the bottom of the experimental charge. Neither olivines (typically >100
194 μm) nor glasses are zoned and are compositionally homogeneous in each experiment. The Fe-Mg
195 exchange coefficient [$K_d(\text{Fe-Mg}) = D(\text{Fe})/D(\text{Mg})$] values between olivine and glass (0.28-0.36)
196 suggest that the experiments closely approached equilibrium (e.g., Filiberto and Dasgupta, 2011).

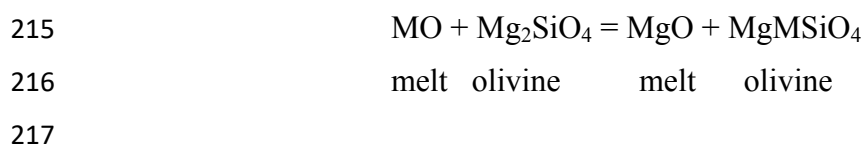
197 *Oxygen fugacity*

198 Our graphite capsule does not buffer fO₂ in systems that contain melt – instead fO₂ is
199 ultimately established in each experimental run by an interplay between Fe³⁺/Fe²⁺, CO₂ solubility
200 and graphite-CO-CO₂ gas equilibria (Pawley et al., 1992; Holloway et al., 1992). Because every
201 bulk composition has a slightly different CO₂ solubility, and different FeO and Fe₂O₃ content,
202 these equilibria can define fO₂ across a window from FMQ-3 to FMQ, and thus it has to be
203 measured for each specific bulk composition. Righter et al. (2009) and Righter et al (2013) used
204 Co-(CoO,MgO) sliding sensor (after Taylor et al., 1992) for shergottite melt compositions to

205 calculate fO_2 for experiments in graphite capsules and they are FMQ-1.5. This relative fO_2 is
206 slightly higher than measured in Y98 (FMQ-2.5 to FMQ-3.5; Shearer et al., 2006; Nakada et al.,
207 2020), but the difference is not significant enough to influence partitioning and this will be
208 discussed in more detail below.

209 *Partition and exchange coefficients*

210 Partition coefficients, $D(M)$ olivine/melt, are the ratio of wt% element M in the olivine /
211 wt% element M in silicate melt, and are known to vary with temperature, pressure, melt
212 composition, and fO_2 . Because $D(M)$'s can be dependent upon subtle melt compositional
213 parameters, and temperature and oxygen fugacity, it is useful to also examine exchange
214 coefficients based on the equilibria such as



218 where $M = V, Cr, Mn, Fe, Co$ or Ni , and the $K_d(M-Mg) = (X_{M_2SiO_4})(X_{MgO}) / (X_{MO})(X_{MgMSiO_4})$
219 which simplifies to $D(M)/D(Mg)$. We examine Ni, Co, Mn, V and Cr partitioning between
220 olivine and melt using both the partition coefficient and exchange coefficients (**Table 3**), to
221 examine the effect of S on partitioning of these elements.

222 The $D(M)$ values for Ni, Co , show a slight decrease and those for V, Cr , and Mn exhibit
223 no variation with increasing S contents (up to 3066 ppm). On the other hand, the $\ln K_d(M-Mg)$
224 values for all five elements decrease with increasing melt S contents (**Fig. 3a,b; Figure 4a,b**).
225 Because partitioning is sometimes dependent upon melt composition or structure, we use the
226 ratio of non-bridging oxygen to tetrahedrally coordinated cations (NBO/T), which is a gauge of
227 melt structure using composition (Mysen, 1991). NBO/T is a simple concept of melt

228 polymerization that can be used to assess variation in melt composition from a polymerized melt
229 like a rhyolite ($NBO/T < 1$) to more depolymerized like peridotitic melt ($NBO/T=2.7$). The
230 $D(M)$ values for Ni decrease slightly with increasing NBO/T , whereas those for Co, V, Cr, and
231 Mn all show little to no correlations (**Fig. 3c,d**). On the other hand, $\ln K_d(M-Mg)$ values for Ni,
232 Mn, V, and Cr all increase with increasing NBO/T and those for Co remain nearly constant (**Fig.**
233 **4c,d**). Examination of $D(M)$ and $\ln K_d(M-Mg)$ variation with NBO/T and Sulfur shows more
234 correlations with NBO/T , and may indicate the importance of melt compositional effects for
235 olivine/melt partitioning of Ni, Co, Mn, V, and Cr. Trends with melt S content and melt
236 composition and/or structure (NBO/T) might be inter-related or co-dependent and so below we
237 look at previous studies for guidance on how to interpret our results.

238

239 **Discussion**

240 *Comparison to previous studies*

241 There have been many systematic studies of trace metal partitioning that can be
242 compared to our new results. When making comparisons, differences in temperature, fO_2 , and
243 melt composition are important to understand. For example, Mallmann and O'Neill (2013)
244 studied V, Mn, and Cr between 1200 and 1530 °C, FMQ-2.85 to +3, with melts including a wide
245 range of FeO contents, but higher Al_2O_3 contents than martian melts, and no sulfur. LeRoux et
246 al. (2011) studied Ni, Co, and Mn at 1310-1500 °C, FMQ-1.5, and for terrestrial basaltic melts
247 with low FeO, high Al_2O_3 , and no S. Gaetani and Grove (1997) carried out experiments at 1350
248 °C, FMQ-1 to -4, on terrestrial basaltic melt compositions with high Al_2O_3 , and low FeO. Their
249 study had variable melt S contents up to ~ 1500 ppm, and also a specified f_{S_2} . Filiberto et al.

250 (2009) examined Ni partitioning at 1300-1420 °C, FMQ-2, for an S-free Gusev (Martian) basalt
251 melt composition. Herd et al. (2009) studied Ni and Co between 1150 and 1290 °C, FMQ-0.5 to
252 -3.0, for three S-free melt compositions (martian, lunar, eucritic). Matzen et al. (2013) studied
253 Ni between 1350 and 1500 °C, 1 bar to 3 GPa, FMQ-1.7, for melts of mid-ocean ridge basalt
254 composition. Hanson and Jones (1998) examined Cr partitioning between olivine and melt for
255 various melt compositions, 1160-1230 °C, and at FMQ and FMQ-4. With a goal of evaluating
256 Ni and Co behavior at high temperatures relevant to a lunar magma ocean, Longhi et al. (2010)
257 studied olivine/melt partitioning to over 2000 °C and FMQ-4. Shearer et al. (2006) studied V at
258 1300-1380 °C, FMQ to FMQ-4.5, and for S-free Yamato 980459 melt compositions. Elardo et
259 al. (2011) measured Ni and Co partitioning in two lunar mantle bulk compositions and at near
260 liquidus conditions between 1 and 3 GPa, and up to 1800 C. Tuff et al. (2010) studied Ni, Co, V,
261 Cr, Mn at 1370-1400 °C, with melts that were medium in FeO and Al₂O₃, FMQ-2 to -3, and
262 variable S. Given the overlap in elements, S-contents and fO₂, their study will be of interest to
263 compare directly to our results. These experiments will be very useful for making comparison of
264 V, Cr, and Mn results at the same T, fO₂, and melt FeO.

265 *Effect of temperature with D(Mg) as a proxy*

266 Previous work has shown that D(Mg) olivine/melt is a good proxy for temperature
267 dependence of partitioning (Jones, 2003, 1995, 1984; Matzen et al., 2013). This is demonstrated
268 with numerous studies for all five elements (**Figure 5**). Positive correlations of D(M) and
269 D(Mg) are observed for Ni, Co, Mn and Cr. Correlations with D(V) are not as clear, but this is
270 due to the strong dependence of D(V) on fO₂ (see next section).

271 *Effect of oxygen fugacity*

272 There is no clear dependence of D(Ni), D(Co), or D(Mn) on oxygen fugacity as might be
273 expected for these three elements that exhibit 2+ valence in fO_2 range of natural magmas.
274 Chromium exhibits two oxidation states in natural magma – 2+ and 3+, yet D(Cr) does not
275 exhibit strong dependence upon fO_2 , as the Cr^{2+}/Cr (tot) varies only slightly across the fO_2 range
276 of natural magmas (Hanson and Jones, 1998; Bell et al., 2017). However, D(V) varies strongly
277 with fO_2 (**Figure 5**), and strong fO_2 dependence has led some previous studies to utilize D(V)
278 olivine/melt as an oxybarometer (Hanson and Jones, 1997; Canil and Fedortchouk, 2001;
279 Mallmann and O'Neill, 2013). When our study is combined with several literature datasets,
280 D(V) clearly varies between 0.001 and 0.4 between FMQ+3 and FMQ-3 (**Figure 5**). The
281 decrease in D(V) at higher fO_2 is caused by a shift from lower valence of V (3+ and 2+) at lower
282 fO_2 to higher valence of V (4 and 3+) at higher fO_2 (e.g., Sutton et al., 2005; Righter et al.,
283 2006).

284 *Effect of melt composition*

285 Melt composition is considered an important variable for Ni, Co, and V partitioning
286 between olivine and melt (Herd et al., 2009; Filiberto et al., 2009; Mallmann and O'Neill, 2013;
287 Tuff and O'Neill, 2010; Matzen et al., 2013). Because of the potential for melt compositional
288 effects, we use the NBO/T melt compositional/structural parameter to assess the effects for each
289 element. D(M) exhibits clear dependence on NBO/T for all five elements (**Figure 5**). For our
290 experiments, K_d (M-Mg) values are also correlated with melt compositions (**Figure 3c, d and 4c,**
291 **d**). For example, K_d (Ni-Mg), K_d (V-Mg), K_d (Cr-Mg), and K_d (Mn-Mg) all increase with
292 increasing NBO/T in the silicate melts (**Fig. 4c, 4d, 6**). In contrast, K_d (Co-Mg) is nearly constant
293 among the samples in our experimental series, (**Fig. 4c, 6**). Thus, predictive expressions for all

294 of these elements will have to include terms for $D(\text{Mg})$, $f\text{O}_2$, and melt composition, and are
295 developed in more detail below with specific studies forming the foundation for comparison.

296 *Effect of S on olivine/melt partition coefficients*

297 To assess the independent contribution of S on the siderophile element partitioning
298 between olivine and melt, we calculate $D(\text{M})$ utilizing predictive expressions whose specific
299 form is based on our assessment in the previous section.

300 Because we are searching for variations in $D(\text{Ni})$ or $D(\text{Co})$ well outside of the
301 experimental error associated with these predictive expressions (typically 10-15%), we will use a
302 simple form to predict $D(\text{Ni})$ and $D(\text{Co})$ in S-free systems to compare to our S-bearing
303 experiments, using $D(\text{Mg})$ and NBO/T as the independent variables. Because Mn does not
304 exhibit valence change across the $f\text{O}_2$ range considered relevant to terrestrial, martian or lunar
305 samples utilized in these studies, and thus it should exhibit similar behavior to Ni and Co, we use
306 these correlations with $D(\text{Mg})$ for Mn as well. Thus, for Ni, Co, and Mn we use $D(\text{Ni}) = a$
307 $D(\text{Mg}) + b (\text{NBO}/\text{T}) + d$, calibrated with S-free experiments that were carried out at otherwise
308 similar conditions (Ni and Co: Longhi et al., 2010; LeRoux et al., 2011; Tuff and O'Neill, 2010;
309 Herd et al., 2009; Filiberto et al., 2009; Elardo et al., 2011; Mn: Tuff and O'Neill, 2010;
310 Mallmann and O'Neill, 2013; LeRoux et al., 2011; and Longhi et al., 2010). Previous studies
311 have adequately modelled $D(\text{Ni})$ and $D(\text{Co})$ as a function of $D(\text{Mg})$ (Jones, 1995; Matzen et al.,
312 2014; Herd et al., 2009).

313 V and Cr both show dependence upon $D(\text{Mg})$ and NBO/T like Ni, Co, and Mn. In
314 addition, studies have shown that $D(\text{V})$ is dependent upon melt composition (Mallmann and
315 O'Neill, 2013). Since these two elements exhibit valence changes over the oxygen fugacities of

316 relevance to terrestrial, martian or lunar samples utilized in these studies, $D(V)$ and $D(Cr)$ will
317 vary with fO_2 . Thus, for V and Cr, we use the expression $D(V) = a D(Mg) + b (NBO/T) + c$
318 $(\Delta FMQ) + d$, calibrated with data from Mallmann and O'Neill (2013), Tuff and O'Neill (2010),
319 and Elardo et al. (201) (For V) and data from experiments of Tuff and O'Neill (2010),
320 Mallmann and O'Neill (2013), Longhi et al. (2010), and Hanson and Jones (1998) (for Cr),
321 across a wide T, fO_2 and melt composition range.

322 Multiple linear regression of $D(M)$ against the two or three variables was done using
323 Sigma Plot 12. Regression results are summarized in **Table 4**, and **Figure 7**. The data used to
324 derive the regression coefficients cover a wide range of temperature, melt composition and fO_2 .
325 The standard error associated with each equation is small, and this error will be critical to
326 evaluating and isolating the effect of sulfur on the olivine/melt partitioning of each element. The
327 difference between the predicted values to the measured values for each of our experiments
328 (**Figure 8**) shows that for most or all of the range of sulfur content, the measured values is within
329 error the same as the predicted value, thus indicating that sulfur does not have a strong effect on
330 partitioning for most elements. However, Co exhibits statistically different values at the highest
331 S contents, indicating that $D(Co)$ can be lower in S-bearing systems compared to S-free. Thus,
332 at the highest S melt values explored here, $D(Co)$ will be slightly lowered, but all other elements
333 – Ni, Mn, Cr, and V – show no variation outside the predicted values in S-free systems.

334 Although our experimental studies suggest that S could slightly reduce partition
335 coefficients of siderophile elements, both $D(Ni)$ and $D(Co)$ are still distinctly greater than one
336 even in our highest S (~3000 ppm) melts. Whether Co can become incompatible depends on
337 how much sulfur is dissolved into the melt, at what temperature, and whether the melts are
338 sulfide saturated. There is evidence from both bulk S and highly siderophile elements that

339 martian melts are sulfide under-saturated (Jones et al., 2003; Righter et al., 2009). However,
340 putting this data aside for a moment, we calculate S content at sulfide saturation to illustrate the
341 potential effect on D(Co) olivine/melt of the highest possible melt S contents. For example, if
342 shergottitic liquids are sulfide saturated in their mantle source, contain >4000 ppm S, and
343 liquidus olivines crystallize at a temperature of ~1450-1500 C, these conditions could push
344 D(Co) to values near or below 1. To test under what conditions D(Co) becomes <1, we have
345 added our S-bearing dataset, as well as S-bearing experiments from Gaetani and Grove (1997)
346 and Tuff and O'Neill (2010), to the regression analysis, and a sulfur term to quantify the effect of
347 dissolved S on D(Co). The equation has the form: $D(\text{Co}) = a D(\text{Mg}) + b(\text{NBO}/\text{T}) + d (\text{ppm S}) +$
348 e , and results in $a = 0.495$, $b = -0.311$, $d = -0.0000824$, $e = 0.843$, with standard error = 0.22
349 (**Table 4**). Application of this equation to martian primary liquids (NBO/T = 1.5, D(Mg) = 2.5)
350 results in $D(\text{Co}) < 1$ if S contents are >8000 ppm. These values are a factor of ~4 higher than
351 measured in primitive martian basalts (1600-2700 ppm S; Ding et al., 2015; Righter et al., 2009
352 and references within), and are 2 times higher than S contents expected if such melts were
353 sulfide saturated in their source (~ 4000 ppm). Therefore, dissolved sulfur is not a realistic way
354 to lower D(Co), even under high S, sulfide saturated conditions.

355

356 **Conclusions and implications**

357 This investigation demonstrates that dissolved S in melts has minimal to no effect on the
358 olivine/melt partitioning of Ni, Co, Mn, V and Cr. Only at high S contents of ~3000 ppm or
359 higher is there a discernable difference in partitioning for Co. These results are essentially
360 consistent with Tuff and O'Neill (2010) whose results suggest that S in the silicate melt has a
361 barely discernible effect on Fe, Co and Ni partition coefficients. Furthermore, they did not

362 recognize detectable effects on Cr, Mn and V. Considering S solubility for primitive martian
363 melts (such as Y-980459) can be as high as ~4000 ppm within a range of reasonable shergottite
364 magmatic conditions (Righter et al., 2009), the olivine/melt partition coefficients for these five
365 elements will only be affected at near sulfide saturation conditions; S contents in sulfide-under-
366 saturated martian liquids are typically not high enough (~1500-2000 ppm) to affect the
367 partitioning.

368 If a change in olivine/melt compatibility is not responsible for the Ni and Co systematics
369 in shergottite olivine, another mechanism or process is causing the apparent incompatibility of
370 Co in shergottite olivines. The de-coupling of Ni and Co is also observed in lunar and terrestrial
371 igneous suites (Sobolev et al., 2007; Karner et al., 2003; Papike et al., 1999), suggesting that
372 finding a solution to the martian sample suite might have wider implications for planetary
373 basalts. Lower oxygen fugacity cannot be an explanation because studies have shown that
374 neither $D(\text{Ni})$ nor $D(\text{Co})$ olivine/melt are dependent upon $f\text{O}_2$ (e.g., **Figure 5**). High
375 temperatures can cause lowering of $D(\text{Ni})$ and $D(\text{Co})$, but even as Longhi et al. (2010) show, the
376 temperatures required are ~ 2000 °C, which are superliquidus for the shergottite or primary
377 martian mantle melts. Changes during fractionation might be called upon to affect the behavior
378 of Co relative to Ni, but the partitioning of these elements would be controlled by clinopyroxene
379 and spinel as other magmatic phases, both of which are hosts for Ni and Co and thus exhibit
380 compatible behavior as well (Righter et al., 2006; Dygert et al., 2014). An additional possible
381 mechanism is a difference in diffusion behavior between Co and Ni in olivine at these
382 conditions. There is diffusion data for both elements that indicates they have very similar
383 diffusion coefficients (Morioka, 1980; 1981), so a diffusion-controlled mechanism is unrealistic

384 as well. Thus, changes in Ni or Co behavior due to fO_2 , temperature, fractionation, or diffusion
385 are not viable explanations.

386 One possibility, suggested by Herd et al. (2009), is that magma mixing may have altered
387 the concentrations of Ni and Co, leading to the apparent incompatible behavior. Shearer et al.
388 (2013) and Usui et al. (2008) suggested the possibility that Y98 olivine cores are xenocrystic.
389 This idea is supported by the presence of xenocrysts in many of the olivine-phyric shergottites
390 (e.g., Castle et al., 2020). Another possibility would require assimilation of a Co-rich material
391 into the shergottite primary liquids after the initial crystallization of olivine, thus causing an
392 apparent incompatibility of Co. Such Co-rich material on Mars is apparently not common, but
393 has been identified in exploration of the Gale Crater region of Mars (Lanza et al., 2016; Berger et
394 al., 2017). Co-rich (~300 ppm Co) and Mn-rich (~3.5 wt.%) deposits have been documented
395 there, associated with hydrothermal activity and oxidation, and the possible presence of oxides.
396 The positive correlation of Co and Mn in olivines and bulk shergottites (and negative correlation
397 with Ni) might support such an idea. A third possibility is that the Ni and Co trends documented
398 in the shergottite olivines are due to possible kinetic crystallization effects (e.g., Kennedy et al.,
399 1993; Papike et al., 1999; Hagerty et al., 2006; Albarede and Bottinga, 1972). All three of these
400 possibilities could be fruitful avenues for future investigations.

401 **Implications**

402 Our partitioning results, in combination with previously published data, show that
403 dissolved sulfur does not affect olivine/melt partitioning of Ni, Mn, Cr, or V, but might have a
404 small effect on Co. However, nearly 8000 ppm of sulfur would be required in martian primary
405 melts for Co to become incompatible ($D(\text{Co}) < 1$), 2 times higher than those of a sulfide saturated
406 melt at the (P,T) conditions of a martian mantle source region. Therefore, the anomalous

407 incompatible behavior observed in these primary magma suites must be due to another
408 mechanism. High temperature, oxygen fugacity, and diffusion are not viable mechanisms, but
409 magma mixing, assimilation, or kinetic crystallization effects remain possibilities.

410 **Acknowledgements**

411 This research was supported by an RTOP to KR from Mars Fundamental Research
412 program, and support from the NASA Planetary Science Directorate (KR), the NASA
413 Postdoctoral Program (TU), Emerging Worlds and Mars Fundamental Research programs (CKS)
414 and the Lunar and Planetary Institute (CKS). We are indebted to Loan Le and Anne Peslier for
415 their technical expertise and assistance in the experimental and analytical laboratories,
416 respectively. We are also grateful for the reviews of V. le Roux and an anonymous reviewer for
417 their helpful constructive comments.

418

419 **References:**

420 Albarede, F. and Bottinga, Y. (1972) Kinetic disequilibrium in trace element partitioning
421 between phenocrysts and host lava. *Geochimica et Cosmochimica Acta* 36, 141-156.

422 Beattie, P., Ford, C., and Russell, D. (1991) Partition coefficients for olivine-melt and
423 orthopyroxene-melt systems. *Contributions to Mineralogy and Petrology* 109, 212-224.

424 Bell, A.S., Shearer, C., Burger, P., Ren, M., Newville, M., and Lanzirotti, A. (2017) Quantifying
425 and correcting the effects of anisotropy in XANES measurements of chromium valence in
426 olivine: Implications for a new olivine oxybarometer. *American Mineralogist* 102, 1165-
427 1172.

- 428 Berger, J.A., Schmidt, M.E., Gellert, R., Boyd, N.I., Desouza, E.D., Flemming, R.L., Izawa,
429 M.R., Ming, D.W., Perrett, G.M., Rampe, E.B., and Thompson, L.M. (2017) Zinc and
430 germanium in the sedimentary rocks of Gale Crater on Mars indicate hydrothermal
431 enrichment followed by diagenetic fractionation. *Journal of Geophysical Research:*
432 *Planets* 122, 1747-1772.
- 433 Canil, D. and Fedortchouk, Y. (2001) Olivine–liquid partitioning of vanadium and other trace
434 elements, with applications to modern and ancient picrites. *The Canadian Mineralogist* 39,
435 319-330.
- 436 Castle, N., Kuehl, E., Jones, J., and Treiman, A. (2020) Multiple origins of xenoliths and
437 xenocrysts in the Elephant Moraine 79001 Lithology A olivine-phyric
438 shergottite. *Meteoritics & Planetary Science* 55, 3-19.
- 439 Collinet, M., Médard, E., Charlier, B., Vander Auwera, J., and Grove, T.L. (2015) Melting of the
440 primitive Martian mantle at 0.5–2.2 GPa and the origin of basalts and alkaline rocks on
441 Mars. *Earth and Planetary Science Letters* 427, 83-94.
- 442 Ding, S., Dasgupta, R., Lee, C.T.A. and Wadhwa, M. (2015) New bulk sulfur measurements of
443 Martian meteorites and modeling the fate of sulfur during melting and crystallization–
444 Implications for sulfur transfer from Martian mantle to crust–atmosphere system. *Earth and*
445 *Planetary Science Letters* 409, 157-167.
- 446 Dreibus, G., Palme, H., Rammensee, W., Spettel, B., Weckwerth, G., and Wänke, H. (1982)
447 Composition of shergotty parent body: Further evidence for a two component model of
448 planet formation. *Lunar and Planetary Science Conference XIII*, 186-187.

- 449 Dreibus, G., Spettel, B., Haubold, R., Jochum, K.P., Palme, H., Wolf, D., and Zipfel, J. (2000)
450 Chemistry of a new shergottite: Sayh al Uhaymir 005. *Meteoritics and Planetary Science*
451 Supplement, 35, A49.
- 452 Dygert, N., Liang, Y., Sun, C., and Hess, P. (2014) An experimental study of trace element
453 partitioning between augite and Fe-rich basalts. *Geochimica et Cosmochimica Acta* 132,
454 170-186.
- 455 Elardo, S.M., Draper, D.S., and Shearer Jr, C.K. (2011) Lunar Magma Ocean crystallization
456 revisited: Bulk composition, early cumulate mineralogy, and the source regions of the
457 highlands Mg-suite. *Geochimica et Cosmochimica Acta* 75, 3024-3045.
- 458 Filiberto, J. and Dasgupta, R. (2011) Fe²⁺-Mg partitioning between olivine and basaltic melts:
459 Applications to genesis of olivine-phyric shergottites and conditions of melting in the
460 Martian interior. *Earth and Planetary Science Letters* 304, 527-537.
- 461 Filiberto, J., Treiman, A.H., and Le, L. (2008) Crystallization experiments on a Gusev
462 Adirondack basalt composition. *Meteoritics & Planetary Science* 43, 1137-1146.
- 463 Filiberto, J., Jackson, C., Le, L., and Treiman, A.H. (2009) Partitioning of Ni between olivine
464 and an iron-rich basalt: Experiments, partition models, and planetary implications. *American*
465 *Mineralogist* 94, 256-261.
- 466 Filiberto J., Musselwhite D., Gross J., Burgess K., Le L., and Treiman A.H. (2010) Experimental
467 petrology, crystallization history and parental magma characteristics of olivine - phyrlic
468 shergottite NWA 1068: Implications for the petrogenesis of “enriched” olivine - phyrlic
469 shergottites. *Meteoritics & Planetary Science* 45, 1258–1270.

- 470 Franz, H.B., Kim, S.T., Farquhar, J., Day, J.M., Economos, R.C., McKeegan, K.D., Schmitt,
471 A.K., Irving, A.J., Hoek, J. and Dottin III, J. (2014) Isotopic links between atmospheric
472 chemistry and the deep sulphur cycle on Mars. *Nature* 508, 364-368.
- 473 Gaetani, G.A. and Grove, T.L. (1997) Partitioning of moderately siderophile elements among
474 olivine, silicate melt, and sulfide melt: Constraints on core formation in the Earth and
475 Mars. *Geochimica et Cosmochimica Acta* 61, 1829-1846.
- 476 Goodrich, C.A. and Delaney, J.S. (2000) Fe/Mg–Fe/Mn relations of meteorites and primary
477 heterogeneity of primitive achondrite parent bodies. *Geochimica et Cosmochimica Acta* 64,
478 149-160.
- 479 Greshake, A., Fritz, J., and Stöffler, D. (2004) Petrology and shock metamorphism of the olivine-
480 phytic shergottite Yamato 980459: Evidence for a two-stage cooling and a single-stage
481 ejection history. *Geochimica et Cosmochimica Acta* 68, 2359-2377.
- 482 Gross J., Treiman A.H., Filiberto J., and Herd C.D.K. (2011) Primitive olivine - phytic
483 shergottite NWA 5789: Petrography, mineral chemistry, and cooling history imply a magma
484 similar to Yamato - 980459. *Meteoritics & Planetary Science* 46, 116–133.
- 485 Hagerty, J.J., Shearer, C.K., Vaniman, D.T., and Burger, P.V. (2006) Identifying the effects of
486 petrologic processes in a closed basaltic system using trace-element concentrations in
487 olivines and glasses: Implications for comparative planetology. *American Mineralogist* 91,
488 1499-1508.
- 489 Hanson, B. and Jones, J.H. (1997) The contrasting partitioning behavior of V and Cr into olivine.
490 *Eos Transactions AGU* **78**, 335.

- 491 Hanson, B. and Jones, J.H. (1998) The systematics of Cr³⁺ and Cr²⁺ partitioning between olivine
492 and liquid in the presence of spinel. American Mineralogist 83, 669-684.
- 493 Herd, C.D., Dwarzski, R.E., and Shearer, C.K. (2009) The behavior of Co and Ni in olivine in
494 planetary basalts: An experimental investigation. American Mineralogist 94, 244-255.
- 495 Herzberg, C., Vidito, C., and Starkey, N.A. (2016) Nickel–cobalt contents of olivine record
496 origins of mantle peridotite and related rocks. American Mineralogist 101, 1952-1966.
- 497 Holloway, J.R., Pan, V., and Gudmundsson, G. (1992) High-pressure fluid-absent melting
498 experiments in the presence of graphite: oxygen fugacity, ferric/ferrous ratio and dissolved
499 CO₂. European Journal of Mineralogy 4, 105-114.
- 500 Holzheid, A. and Grove, T. L. (2002) Sulfur saturation limits in silicate melts and their
501 implications for core formation scenarios for terrestrial planets. American Mineralogist 87,
502 227-237.
- 503 Humayun, M., Qin, L., and Norman, M.D. (2004) Geochemical evidence for excess iron in
504 the mantle beneath Hawaii. Science 306, 91-94.
- 505 Jones, J.H. (1984) Temperature- and pressure-independent correlations of olivine/liquid
506 partition coefficients and their application to trace element partitioning. Contributions
507 to Mineralogy and Petrology 88, 126-132.
- 508 Jones, J.H. (1995) Experimental trace element partitioning. In T.J. Ahrens, Ed., Rock Physics &
509 Phase Relations: A Hand Book of Physical Constants, p. 73-104, American Geophysical
510 Union, Washington, DC.

- 511 Jones, J.H. (2003) A liquidus geothermometer for SNC, lunar, and eucritic magmas. Lunar and
512 Planetary Science XXXIV, Abstract #1130.
- 513 Jones, J.H., Neal, C.R., and Ely, J.C. (2003) Signatures of the highly siderophile elements in the
514 SNC meteorites and Mars: a review and petrologic synthesis. *Chemical Geology* 196, 5-25.
- 515 Karner, J., Papike, J.J., and Shearer, C.K. (2003) Olivine from planetary basalts: Chemical
516 signatures that indicate planetary parentage and those that record igneous setting and
517 process. *American Mineralogist* 88, 806-816.
- 518 Kennedy, A.K., Lofgren, G.E., and Wasserburg, G.J. (1993) An experimental study of trace
519 element partitioning between olivine, orthopyroxene and melt in chondrules: equilibrium
520 values and kinetic effects. *Earth and Planetary Science Letters* 115, 177-195.
- 521 Lanza, N.L., Wiens, R.C., Arvidson, R.E., Clark, B.C., Fischer, W.W., Gellert, R., ... and Rice,
522 M. S. (2016) Oxidation of manganese in an ancient aquifer, Kimberley formation, Gale
523 crater, Mars. *Geophysical Research Letters* 43, 7398-7407.
- 524 Laurenz, V., Fonseca, R.O., Ballhaus, C., Jochum, K.P., Heuser, A., and Sylvester, P.J. (2013)
525 The solubility of palladium and ruthenium in picritic melts: 2. The effect of
526 sulfur. *Geochimica et Cosmochimica Acta* 108, 172-183.
- 527 Lee, C.T.A., Brandon, A.D., and Norman, M. (2003) Vanadium in peridotites as a proxy for
528 paleo-fO₂ during partial melting: prospects, limitations, and implications. *Geochimica et*
529 *Cosmochimica Acta* 67, 3045-3064.

- 530 Le Roux, V., Dasgupta, R., and Lee, C.T. (2011) Mineralogical heterogeneities in the Earth's
531 mantle: constraints from Mn, Co, Ni and Zn partitioning during partial melting. Earth and
532 Planetary Science Letters 307, 395-408.
- 533 Le Voyer, M., Hauri, E.H., Cottrell, E., Kelley, K.A., Salters, V.J., Langmuir, C.H., Hilton, D.R.,
534 Barry, P.H. and Fűri, E. (2019) Carbon Fluxes and Primary Magma CO₂ Contents Along the
535 Global Mid - Ocean Ridge System. *Geochemistry, Geophysics, Geosystems* 20, 1387-1424.
- 536 Li, C., Ripley, E.M., and Mathez, E.A. (2003) The effect of S on the partitioning of Ni between
537 olivine and silicate melt in MORB. *Chemical Geology* 201, 295-306.
- 538 Libourel, G. (1999) Systematics of calcium partitioning between olivine and silicate melt:
539 implications for melt structure and calcium content of magmatic olivines. *Contributions to*
540 *Mineralogy and Petrology* 136, 63-80.
- 541 Longhi, J., Durand, S.R., and Walker, D. (2010) The pattern of Ni and Co abundances in lunar
542 olivines. *Geochimica et Cosmochimica Acta* 74, 784-798.
- 543 Mallmann, G. and O'Neill, H.St.C. (2013) Calibration of an empirical thermometer and
544 oxybarometer based on the partitioning of Sc, Y and V between olivine and silicate
545 melt. *Journal of Petrology* 54, 933-949.
- 546 Matzen, A.K., Baker, M.B., Beckett, J.R. and Stolper, E.M. (2013) The temperature and pressure
547 dependence of nickel partitioning between olivine and silicate melt. *Journal of Petrology* 54,
548 2521-2545.
- 549 Morioka, M. (1980) Cation diffusion in olivine—I. Cobalt and magnesium. *Geochimica et*
550 *Cosmochimica Acta* 44, 759-762.

- 551 Morioka, M. (1981) Cation diffusion in olivine—II. Ni-Mg, Mn-Mg, Mg and Ca. *Geochimica et*
552 *Cosmochimica Acta* 45 1573-1580.
- 553 Mysen, B.O. (1991) Relations between structure, redox equilibria of iron, and properties of
554 magmatic liquids. In L.L. Perchuk, Ed., *Physical Chemistry of Magmas*, p. 41-98, Springer,
555 New York, NY.
- 556 Nakada, R., Usui, T., Ushioda, M., and Takahashi Y. (2020) Vanadium micro-XANES
557 determination of oxygen fugacity in olivine-hosted glass inclusion and groundmass glasses of
558 martian primitive basalt Yamato 980459. *American Mineralogist* 105, 1695-1703.
- 559 Papike, J.J. (1998) *Comparative Planetary Mineralogy: Chemistry of Melt- Derived Pyroxene,*
560 *Feldspar, and Olivine.* In J.J. Papike, Ed., *Planetary Materials*, 36, 7-01 - 7-12. Reviews in
561 *Mineralogy and Geochemistry*, Mineralogical Society of America, Chantilly, Virginia.
- 562 Papike, J.J., Fowler, G.W., Adcock, C.T., and Shearer, C.K. (1999) Systematics of Ni and Co in
563 olivine from planetary melt systems: Lunar mare basalts. *American Mineralogist* 84, 392-
564 399.
- 565 Papike, J.J., Karner, J.M., Shearer, C.K., and Burger, P.V. (2009) Silicate mineralogy of martian
566 meteorites. *Geochimica et Cosmochimica Acta* 73, 7443-7485.
- 567 Pawley, A.R., Holloway, J.R., and McMillan, P.F. (1992) The effect of oxygen fugacity on the
568 solubility of carbon-oxygen fluids in basaltic melt. *Earth and Planetary Science Letters* 110,
569 213-225.

- 570 Pouchou, J.L. and Pichoir, F. (1991) Quantitative analysis of homogeneous or stratified
571 microvolumes applying the model "PAP". In K.G.F.J. Heinrich and D. Newbury, Eds.,
572 Electron Probe Quantitation, p. 31-75, Springer, Boston, MA.
- 573 Rapp, J. F., Draper, D. S., and Mercer, C. M. (2013) Anhydrous liquid line of descent of
574 Yamato - 980459 and evolution of Martian parental magmas. *Meteoritics & Planetary*
575 *Science* 48, 1780-1799.
- 576 Righter, K., Leeman, W.P., and Hervig, R.L. (2006) Partitioning of Ni, Co and V between
577 spinel-structured oxides and silicate melts: Importance of spinel composition. *Chemical*
578 *Geology* 227, 1-25.
- 579 Righter, K., Pando, K., and Danielson, L.R. (2009) Experimental evidence for sulfur-rich
580 martian magmas: Implications for volcanism and surficial sulfur sources. *Earth and Planetary*
581 *Science Letters* 288, 235-243.
- 582 Righter, K., Danielson, L.R., Pando, K., Morris, R.V., Graff, T.G., Agresti, D.G., Martin, A.M.,
583 Sutton, S.R., Newville, M., and Lanzirotti, A. (2013) Redox systematics of martian magmas
584 with implications for magnetite stability. *American Mineralogist* 98, 616-628.
- 585 Sato, H. (1977) Nickel content of basaltic magmas: identification of primary magmas and a
586 measure of the degree of olivine fractionation. *Lithos* 10, 113-120.
- 587 Shirai, N. and Ebihara, M. (2004) Chemical characteristics of a Martian meteorite, Yamato
588 980459. *Antarctic Meteorite Research* 17, 55-67.
- 589 Shearer, C.K. and Papike, J.J. (2005) Early crustal building processes on the moon: Models for
590 the petrogenesis of the magnesian suite. *Geochimica et Cosmochimica Acta* 69, 3445-3461.

- 591 Shearer, C.K., Papike, J.J., Simon, S.B., Shimizu, N., Yurimoto, H., and Sueno, S. (1990) Ion
592 microprobe studies of trace elements in Apollo 14 volcanic glass beads: Comparisons to
593 Apollo 14 mare basalts and petrogenesis of picritic magmas. *Geochimica et Cosmochimica*
594 *Acta* 54, 851-867.
- 595 Shearer, C. K., Papike, J. J., & Layne, G. D. (1996) Deciphering basaltic magmatism on the
596 Moon from the compositional variations in the Apollo 15 very low-Ti picritic magmas.
597 *Geochimica et Cosmochimica Acta* 60, 509-528.
- 598 Shearer, C.K., McKay, G.A, Papike, J.J., and Karner, J.M. (2006) Valence state partitioning of
599 vanadium between olivine-liquid: Estimates of the oxygen fugacity of Y980459 and
600 application to other olivine-phyric martian basalts. *American Mineralogist* 91, 1657-1663.
- 601 Shearer, C.K., Aaron, P.M., Burger, P.V., Guan, Y., Bell, A.S., and Papike, J.J. (2013)
602 Petrogenetic linkages among fO_2 , isotopic enrichments-depletions and crystallization history
603 in Martian basalts. Evidence from the distribution of phosphorus in olivine megacrysts.
604 *Geochimica et Cosmochimica Acta* 120, 17-38.
- 605 Snetsinger, K.G., Bunch, T.E., and Keil, K. (1968) Electron microprobe analysis of vanadium in
606 the presence of titanium. *American Mineralogist: Journal of Earth and Planetary*
607 *Materials* 53, 1770-1773.
- 608 Sobolev, A.V., Hofmann, A.W., Kuzmin, D.V., Yaxley, G.M., Arndt, N.T., Chung, S.L.,
609 Danyushevsky, L.V., Elliott, T., Frey, F.A., Garcia, M.O. and Gurenko, A.A. (2007) The
610 amount of recycled crust in sources of mantle-derived melts. *Science* 316, 412-417.

- 611 Takahashi, E. (1978) Partitioning of Ni^{2+} , Co^{2+} , Fe^{2+} , Mn^{2+} and Mg^{2+} between olivine and
612 silicate melts: compositional dependence of partition coefficient. *Geochimica et*
613 *Cosmochimica Acta* 42, 1829-1844.
- 614 Taylor, J.R., Wall, V.J., and Pownceby, M.I. (1992) The calibration and application of accurate
615 redox sensors. *American Mineralogist* 77, 284-295.
- 616 Toplis, M.J. (2005) The thermodynamics of iron and magnesium partitioning between olivine
617 and liquid: criteria for assessing and predicting equilibrium in natural and experimental
618 systems. *Contributions to Mineralogy and Petrology* 149, 22-39.
- 619 Tuff, J. and O'Neill, H.St.C. (2010) The effect of sulfur on the partitioning of Ni and other first-
620 row transition elements between olivine and silicate melt. *Geochimica et Cosmochimica*
621 *Acta* 74, 6180-6205.
- 622 Usui, T., McSween Jr, H.Y., and Floss, C. (2008) Petrogenesis of olivine-phyric shergottite
623 Yamato 980459, revisited. *Geochimica et Cosmochimica Acta* 72, 1711-1730.
- 624 Wänke, H. and Dreibus, G. (1986) Geochemical evidence for the formation of the Moon by
625 impact-induced fission of the proto-Earth. In W. K. Hartmann, R. J. Phillips, and G. J.
626 Taylor, Eds., *Origin of the Moon*, p. 649-672, Lunar and Planetary Institute, Houston, TX.
- 627 Zipfel, J., Scherer, P., Spettel, B., Dreibus, G., and Schultz, L. (2000) Petrology and chemistry of
628 the new shergottite Dar al Gani 476. *Meteoritics & Planetary Science* 35, 95-106.
- 629
- 630

631 **Figure Captions**

632 **Figure 1:** Ni and Co concentrations in shergottite olivines showing compatible behavior of Ni
633 with fractionation (or increasing XFe), and incompatible behavior of Co (from Papike et al.,
634 2009; Shearer et al., 2008; Usui et al., 2008). These trends suggest that in shergottite systems Co
635 exhibits incompatibility in olivine, counter to evidence from many partitioning studies that show
636 it is compatible. Usui et al. (2008) also demonstrate Ni and Co incompatibility in high Fo
637 olivines from Y-980459. Error on Ni and Co measurements are smaller than the symbols;
638 arrows also show the direction of differentiation.

639 **Figure 2:** Back scattered electron image of run product from experiment #16, at 0.75 GPa, 1475
640 °C, with sample composition of synthetic Y-980459 melt with 1000 ppm S added. Duration was
641 3 hours, with a 30 minute dwell at 1500 °C before lowering to 1475 °C for olivine growth.

642 **Figure 3: (a,b):** D(M) versus S content [S] of coexisting melt for the experiments in this study.
643 (a) Ni and Co, and (b) Mn, Cr, and V. Hatched line indicates a 1-sigma deviation of each
644 regression line.

645 $D(\text{Ni}) = -0.0003 * [S] + 7.2739$ ($R^2 = 0.0365$);

646 $D(\text{Co}) = -(7 \times 10^{-6}) * [S] + 1.4543$ ($R^2 = 0.0012$);

647 $D(\text{Mn}) = -(4 \times 10^{-6}) * [S] + 0.7313$ ($R^2 = 0.0084$);

648 $D(\text{Cr}) = -(5 \times 10^{-6}) * [S] + 0.5975$ ($R^2 = 0.0483$);

649 $D(\text{V}) = -(4 \times 10^{-6}) * [S] + 0.2243$ ($R^2 = 0.0855$).

650 **(c,d):** D(M) versus NBO/T of coexisting melt for the experiments in this study; (c) Ni and Co,
651 and (d) Mn, Cr, and V. Hatched line indicates a 1-sigma deviation of each regression line.

652 $D(\text{Ni}) = -1.6595 * (\text{NBO}/\text{T}) + 9.3734 (R^2 = 0.036);$

653 $D(\text{Co}) = -0.7374 * (\text{NBO}/\text{T}) + 2.532 (R^2 = 0.4018);$

654 $D(\text{Mn}) = -0.0857 * (\text{NBO}/\text{T}) + 0.8623 (R^2 = 0.1128);$

655 $D(\text{Cr}) = -0.0394 * (\text{NBO}/\text{T}) + 0.6497 (R^2 = 0.0917);$

656 $D(\text{V}) = + 0.0587 * (\text{NBO}/\text{T}) + 0.133 (R^2 = 0.548).$

657 **Figure 4: (a,b):** $\ln K_d(\text{M-Mg})$ versus S content [S] of coexisting melt for the experiments in this
658 study, where M = (a) Ni and Co, and (b) Cr and V. Hatched line indicates a 1-sigma deviation of
659 each regression line.

660 $\ln K_d(\text{Ni-Mg}) = -(1.11 \times 10^{-4}) * [\text{S}] + 0.970 (R^2 = 0.28);$

661 $\ln K_d(\text{Co-Mg}) = -(4.22 \times 10^{-5}) * [\text{S}] - 0.398 (R^2 = 0.282);$

662 $\ln K_d(\text{Mn-Mg}) = -(6.0 \times 10^{-5}) * [\text{S}] - 1.3162 (R^2 = 0.4057);$

663 $\ln K_d(\text{Cr-Mg}) = -(7.58 \times 10^{-5}) * [\text{S}] - 1.52 (R^2 = 0.468);$

664 $\ln K_d(\text{V-Mg}): y = -(8.35 \times 10^{-5}) * [\text{S}] - 2.50 (R^2 = 0.299).$

665 **(c, d):** $\ln K_d(\text{M-Mg})$ versus NBO/T of coexisting melt for the experiments in this study, where M
666 = (c) Ni and Co, and (d) Mn, Cr, and V. Note that the S-rich melts have a lower NBO/T value
667 than S-poor melts. Hatched line indicates a 1-sigma deviation of each regression line.

668 $\ln K_d(\text{Ni-Mg}) = 0.4133 * \text{NBO}/\text{T} + 0.2211 (R^2 = 0.1027);$

669 $\ln K_d(\text{Co-Mg}) = 0.016 * \text{NBO}/\text{T} - 0.4749 (R^2 = 0.0011);$

670 $\ln K_d(\text{Mn-Mg}) = 0.5213 * \text{NBO}/\text{T} - 2.1634 (R^2 = 0.7408);$

671 $\ln K_d(\text{Cr-Mg}) = 0.5706 * \text{NBO/T} - 2.4537$ ($R^2 = 0.7006$);

672 $\ln K_d(\text{V-Mg}): y = 0.8983 * \text{NBO/T} - 3.9291$ ($R^2 = 0.9112$).

673 **Figure 5:** Comparison of $D(\text{Ni})$, $D(\text{Co})$, $D(\text{Mn})$, $D(\text{V})$, and $D(\text{Cr})$ to those from previous studies,
674 examining variations with $D(\text{Mg})$, NBO/T , and relative $f\text{O}_2$ (ΔFMQ).

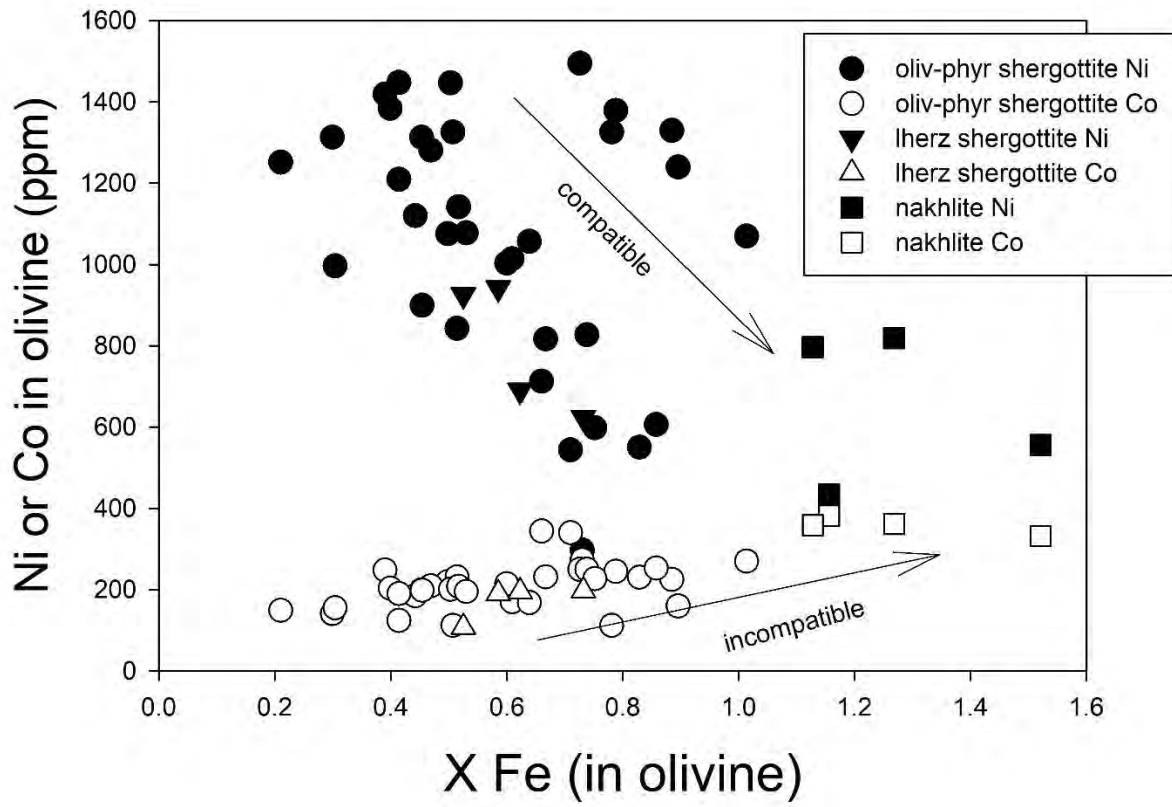
675 **Figure 6:** Comparison of $K_d(\text{Ni-Mg})$, $K_d(\text{Co-Mg})$, $K_d(\text{Mn-Mg})$, $K_d(\text{Cr-Mg})$, and $K_d(\text{V-Mg})$
676 from previous studies, examining variations with NBO/T .

677 **Figure 7:** Comparison of measured vs. predicted $D(\text{Ni})$, $D(\text{Co})$, $D(\text{Mn})$, $D(\text{V})$, and $D(\text{Cr})$
678 olivine/melt. Predicted values were calculated using equations and constants tabulated in Table
679 4.

680 Data sources are listed in the legends, and also summarized in Table 4.

681 **Figure 8:** Difference between measured and calculated $D(\text{M})$ as a function of S content of
682 coexisting melt. $D(\text{M})$ olivine/melt predicted are calculated using equations summarized in Table
683 4. Shaded areas shows 2σ error on the predicted values.

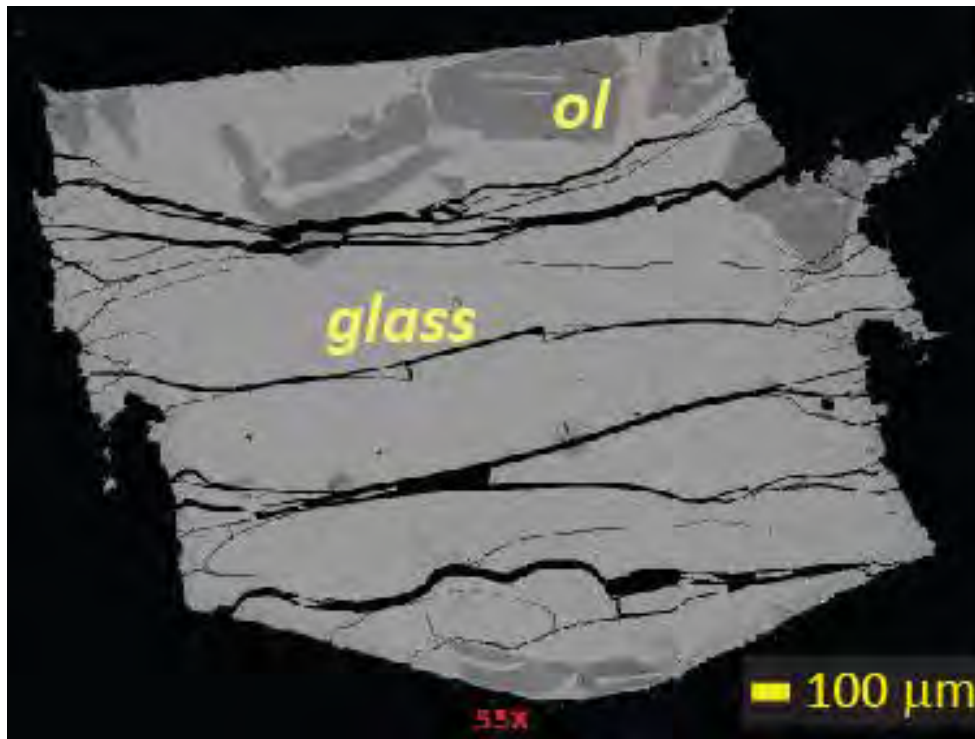
684 **Figure 1**



685

686

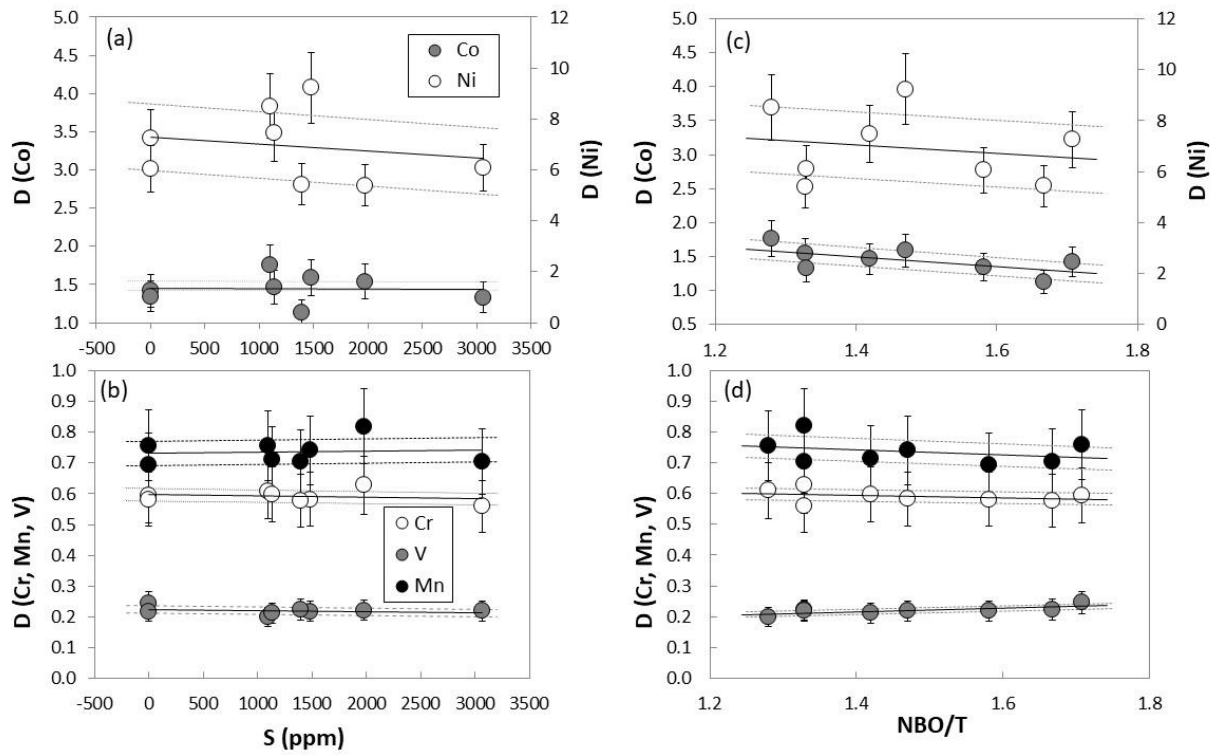
687 **Figure 2**



688

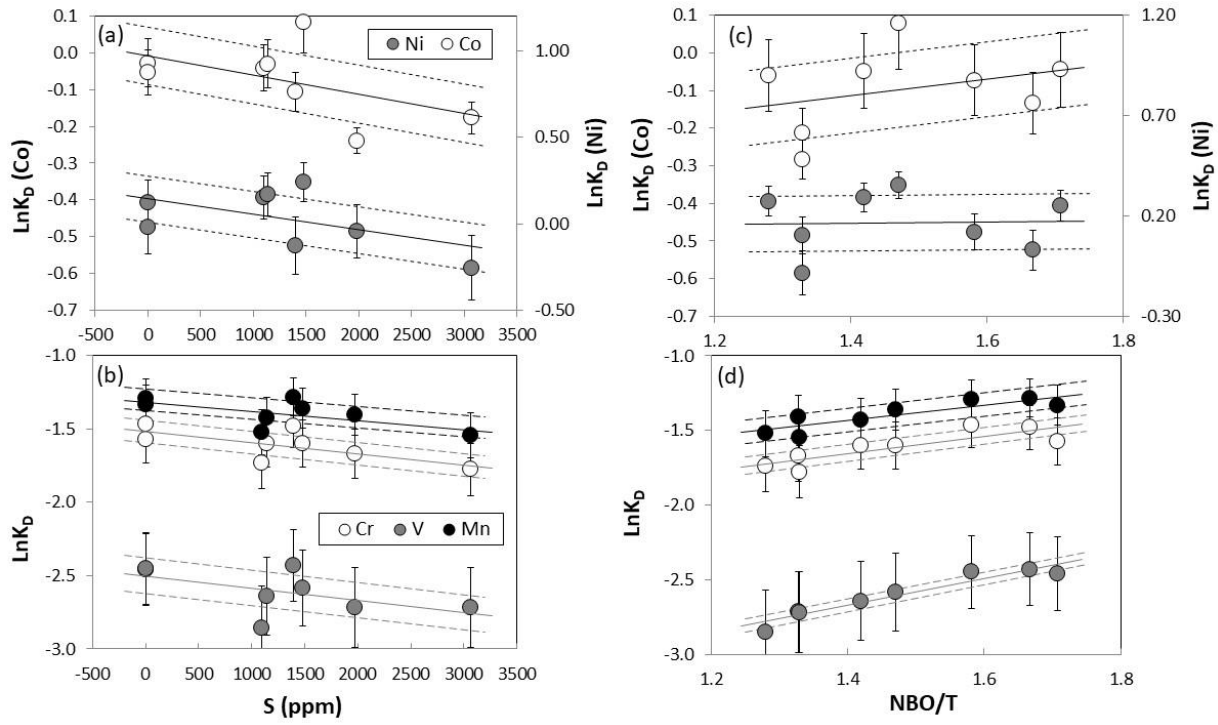
689

690 Figure 3:
691



692
693
694

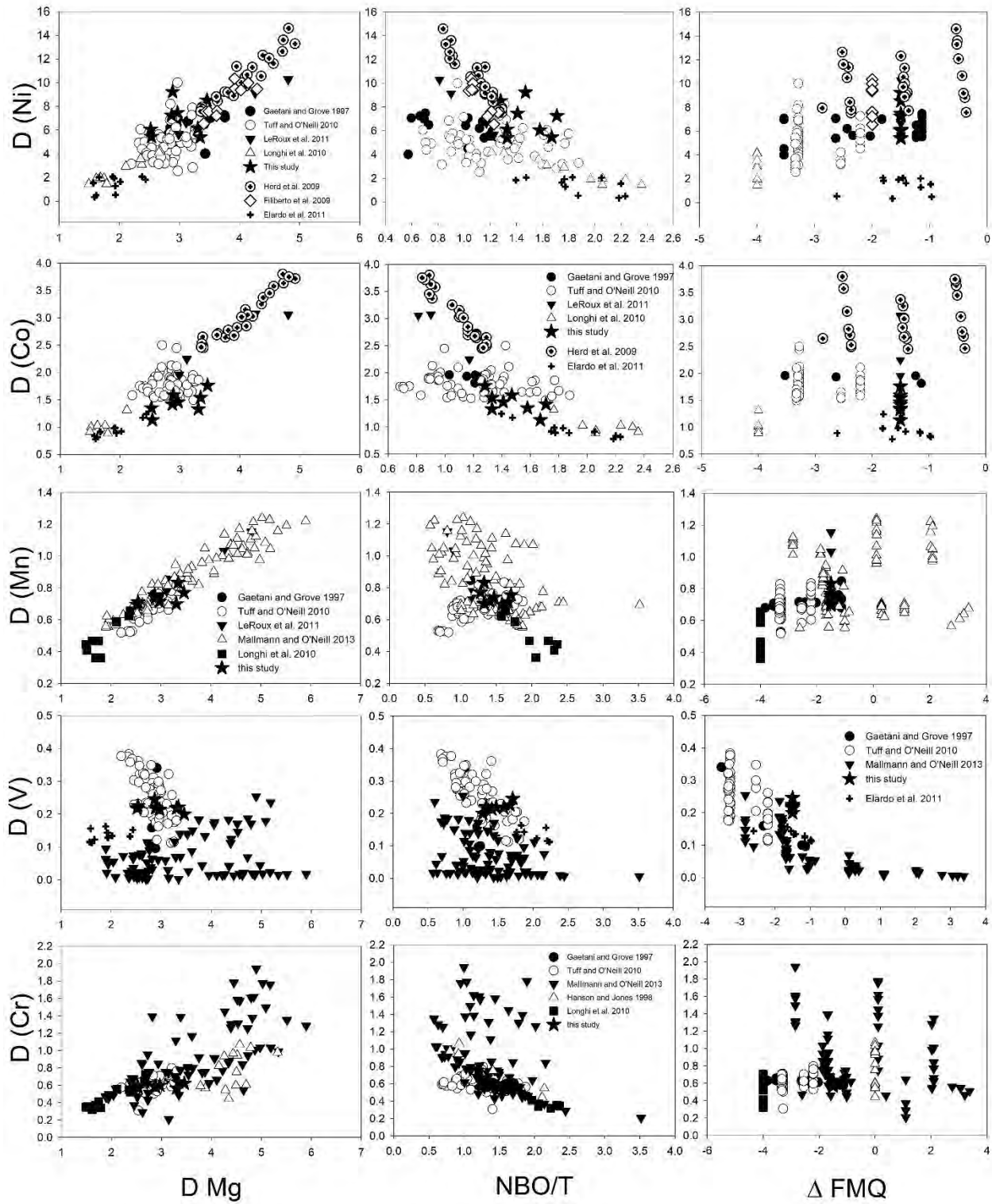
695 Figure 4:



696

697

698 Figure 5:

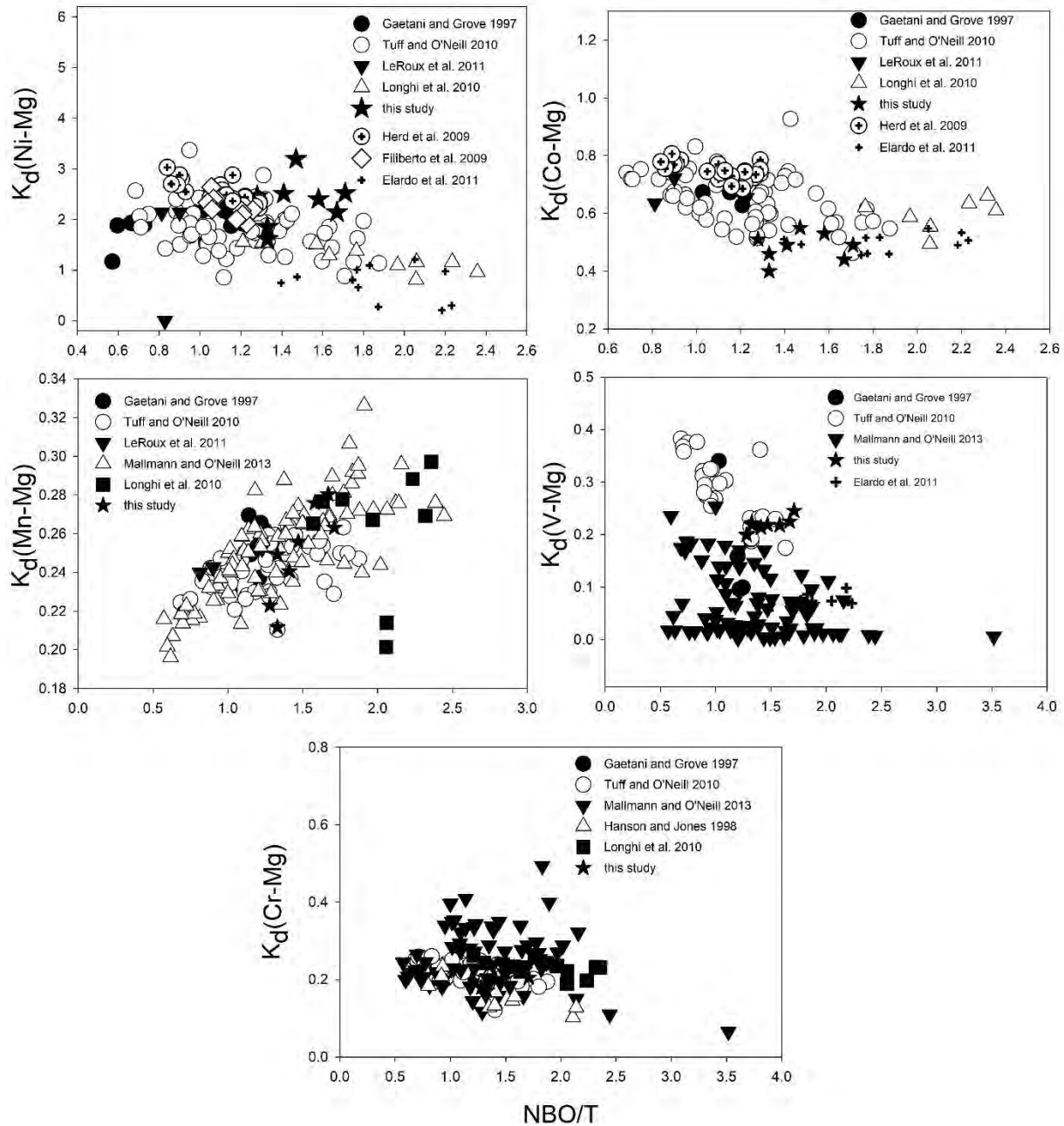


699

700

701

702 Figure 6:

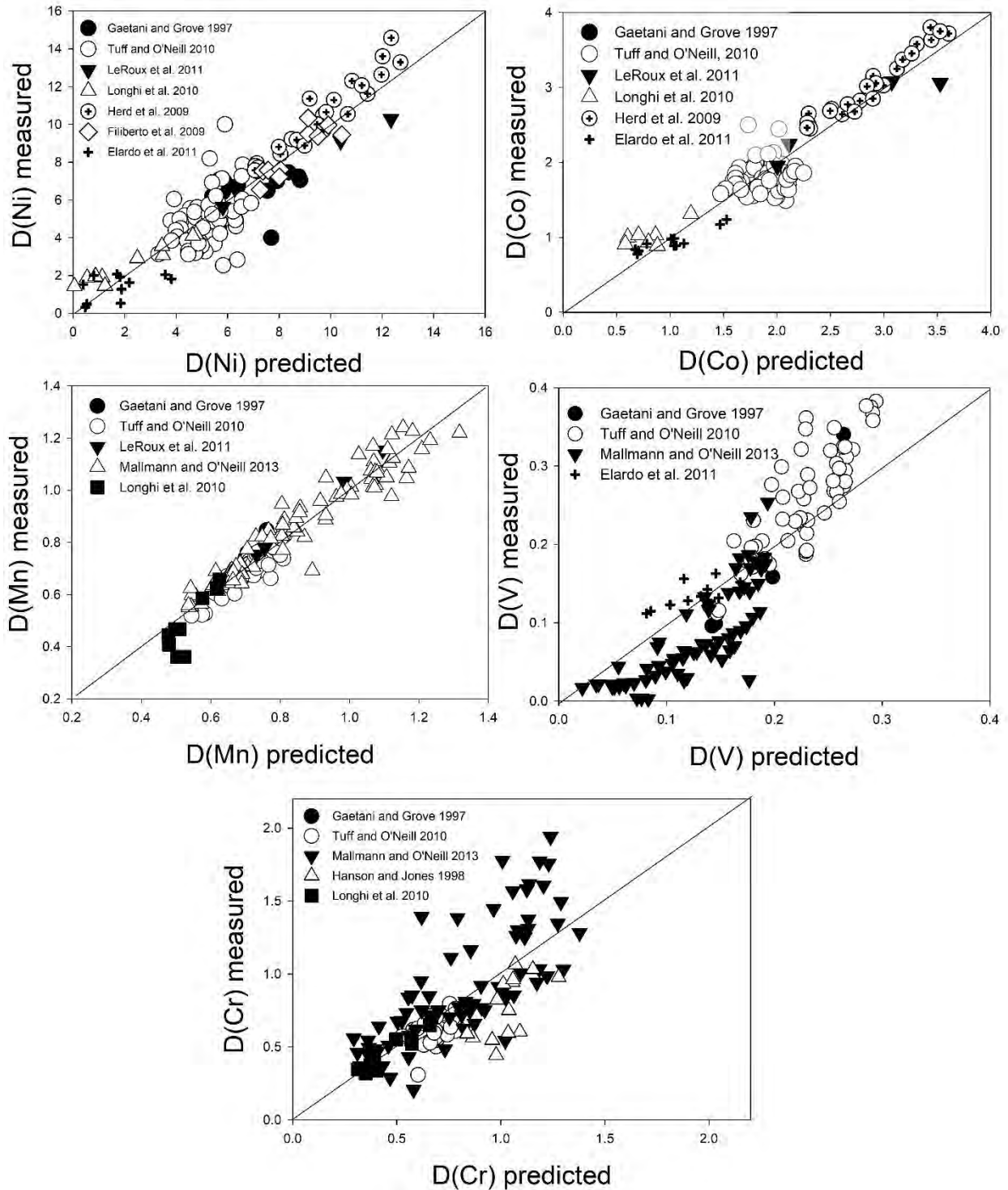


703

704

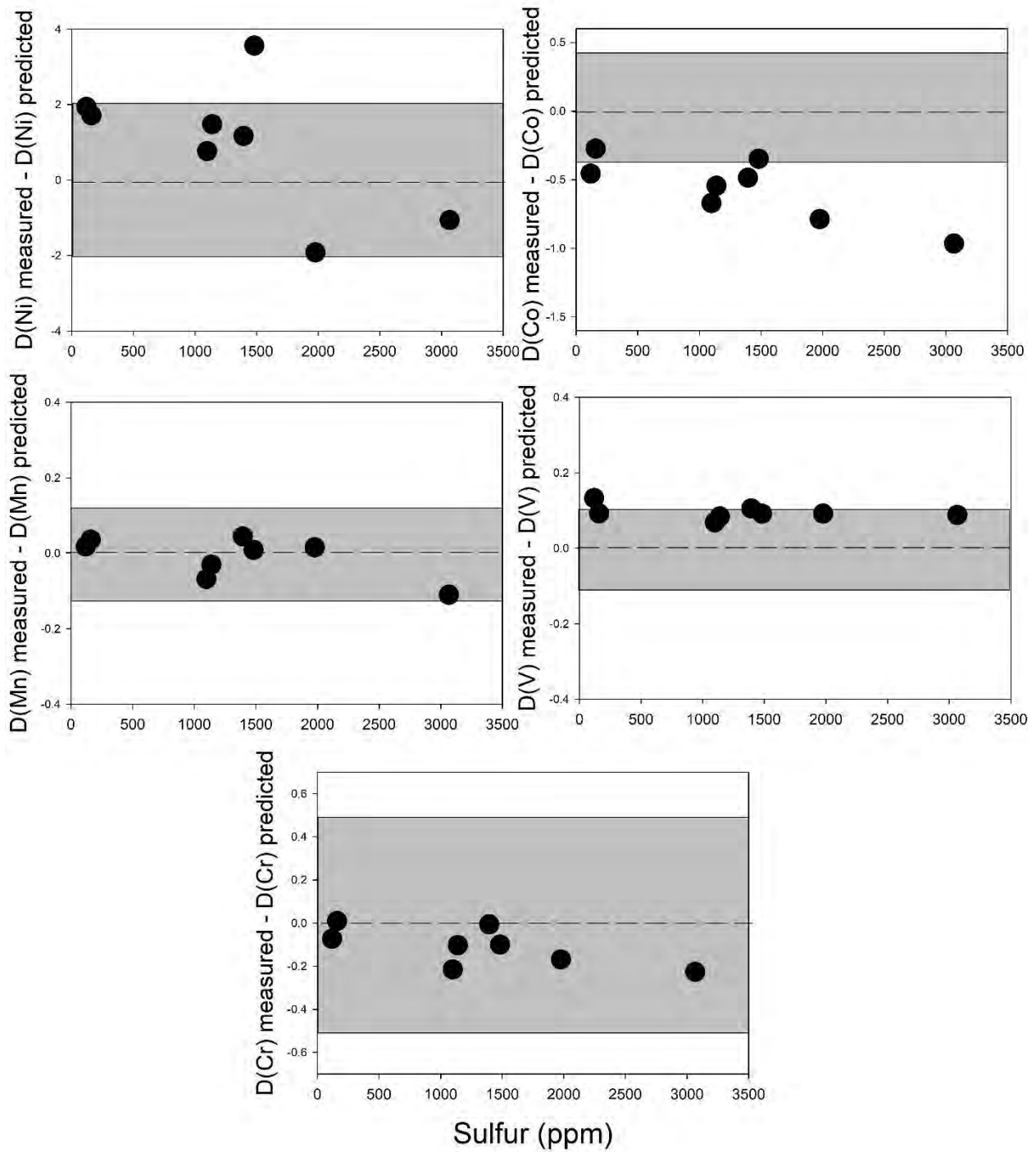
705

706 Figure 7:



707
708

709 Figure 8:



710
711
712

713 **Table 1: Run conditions, electron microprobe and SIMS analyses of glass** (all experiments at 0.75 GPa, with olivine and glass)

714

Run#	Starting	11	14	16	17	22	27	28	29
T (°C)		1500	1475	1475	1475	1450	1450	1450	1475
S added		2000	2000	1000	0	2000	0	1000	3000
% melt		98	93	88	98	85	88	83	86
n		13	12	12	10	12	13	14	12
SiO ₂	49.9	46.81(40)	49.14 (20)	49.69(17)	49.24(43)	50.26(21)	49.74(30)	51.00(24)	50.31(36)
TiO ₂	0.532	0.55(3)	0.55(3)	0.59(1)	0.51(1)	0.67(2)	0.62(3)	0.64(3)	0.62(2)
Al ₂ O ₃	5.17	6.26(12)	6.62(30)	7.14(43)	6.24(6)	7.25(9)	7.03(14)	7.49(13)	7.49(10)
Cr ₂ O ₃	0.659	0.65(3)	0.66(2)	0.67(2)	0.65(3)	0.68(2)	0.68(3)	0.63(2)	0.69(2)
FeO	17.3	16.83(19)	16.84(20)	16.55(30)	16.41(9)	16.70(17)	16.62(23)	16.59(16)	16.69(19)
MnO	0.481	0.45(4)	0.46(3)	0.49(4)	0.46(4)	0.42(3)	0.45(3)	0.48(2)	0.50(5)
MgO	18.7	17.58(32)	15.26(51)	14.82(58)	17.57(14)	12.87(12)	15.33(13)	12.65(19)	13.43(10)
CaO	6.83	6.98(13)	7.33(21)	7.76(17)	6.94(11)	7.98(6)	7.77(7)	8.17(9)	7.96(8)
Na ₂ O	0.651	0.70(3)	0.69(4)	0.78(3)	0.67(4)	1.30(5)	0.71(3)	0.79(3)	0.80(3)
K ₂ O	0.0156	0.024(14)	0.030(13)	0.028(10)	0.025(12)	0.030(13)	0.035(12)	0.038(11)	0.025(13)
P ₂ O ₅	0.29	0.34(5)	0.34(7)	0.36(5)	0.32(4)	0.36(3)	0.33(4)	0.35(4)	0.36(4)
S (ppm)	-	1394(185)	1481(232)	1139(179)	160(131)	1977(267)	119(130)	1098(134)	3066(218)
Cr (ppm)	-	4416(203)	4487(125)	4556(166)	4468(202)	4664(130)	4621(176)	4330(166)	4710(142)
Mn (ppm)	-	3473(305)	3563(198)	3795(276)	3532(337)	3266(211)	3467(257)	3745(186)	3866(374)
Total	100.529	97.45(37)	98.22(45)	99.12(36)	99.08(53)	98.92(34)	99.35(44)	99.06(30)	99.50(46)
NBO/T	-	1.67	1.47	1.42	1.58	1.33	1.71	1.28	1.33
V (SIMS)	-	182(9)	188(10)	192(10)	187(10)	207(11)	201(10)	202(10)	192(10)
Co (SIMS)	-	437(22)	401(20)	385(19)	510(25)	316(16)	447(22)	358(17)	300(15)
Ni (SIMS)	-	71.0(4.0)	56.5(2.8)	56.7(2.8)	56.7(2.8)	39.7(2.0)	51.0(2.5)	43.1(2.2)	54.0(2.7)

715 **Table 2: Olivine EMPA and SIMS analyses**

Run#	11	14	16	17	22	27	28	29
n	11	11	13	11	11	13	15	15
SiO ₂	39.13(10)	39.22(17)	39.21(15)	38.90(7)	38.75(9)	38.69(20)	38.45(26)	38.43(24)
Cr ₂ O ₃	0.37(1)	0.38(1)	0.40(2)	0.38(1)	0.43(1)	0.40(1)	0.39(2)	0.39(2)
FeO	14.72(10)	16.08(24)	16.14(58)	14.77(6)	17.08(44)	15.82(26)	16.04(98)	15.43(74)
MnO	0.32(1)	0.34(1)	0.35(1)	0.32(1)	0.35(2)	0.34(1)	0.37(2)	0.35(2)
MgO	44.60(14)	44.08(29)	44.00(35)	44.31(11)	43.03(43)	44.03(22)	43.76(83)	44.41(67)
CaO	0.17(1)	0.17(1)	0.19(1)	0.18(1)	0.19(1)	0.18(1)	0.17(1)	0.17(1)
NiO	0.049(7)	0.066(12)	0.054(8)	0.044(8)	0.027(10)	0.047(9)	0.047(9)	0.042(10)
CoO	0.063(5)	0.081(7)	0.072(6)	0.087(5)	0.062(8)	0.081(6)	0.080(8)	0.051(5)
Total	99.43(27)	100.43(25)	100.41(39)	98.99(16)	99.91(14)	99.59(17)	99.30(14)	99.26(19)
Si	0.990	0.989	0.989	0.990	0.987	0.984	0.982	0.979
Cr	0.007	0.008	0.008	0.008	0.009	0.008	0.008	0.008
Fe ²⁺	0.312	0.339	0.340	0.314	0.364	0.336	0.343	0.329
Mn	0.0068	0.0073	0.0075	0.0068	0.0075	0.0073	0.0079	0.0076
Mg	1.683	1.657	1.655	1.681	1.634	1.669	1.666	1.687
Ca	0.0047	0.0046	0.0051	0.0050	0.0051	0.0050	0.0047	0.0046
Ni	0.0010	0.0013	0.0011	0.0009	0.0006	0.0010	0.0010	0.0009
Co	0.001	0.002	0.001	0.002	0.001	0.002	0.002	0.001
Total	3.0	3.0	3.0	3.0	3.0	3.0	3.0	3.0
Fo	83.8(1)	82.4(3)	82.3(6)	83.6(1)	81.2(5)	82.6(3)	82.3(1.1)	83.1(9)
Mg #	84.4(1)	83.0(3)	82.9(6)	84.2(1)	81.8(5)	83.2(3)	83.2(3)	83.7(9)
V (SIMS)	41.0(4.0)	41.1(4.1)	41.0(4.0)	40.8(4.1)	45.8(4.6)	49.4(5.0)	40.2(4.0)	41.9(4.2)
Co (EMPA)	493(25)	636(32)	563(28)	686(34)	486(24)	635(32)	629(31)	399(20)
Ni (EMPA)	386(19)	521(26)	423(21)	343(17)	214(11)	369(18)	367(18)	331(16)

716

717

718 **Table 3: D and K_d values**

Run #	27	28	22	17	16	14	29	11
Temp	1450	1450	1450	1475	1475	1475	1475	1500
S (ppm)	0	1000	2000	0	1000	2000	3000	2000
D V	0.25(3)	0.20(3)	0.22(3)	0.22(3)	0.21(3)	0.22(3)	0.22(3)	0.23(3)
D Cr	0.60(4)	0.62(4)	0.63(4)	0.58(4)	0.60(4)	0.58(4)	0.57(4)	0.57(4)
D Mn	0.76(9)	0.77(9)	0.83(9)	0.70(8)	0.71(8)	0.74(8)	0.70(8)	0.71(8)
D Fe	0.95(2)	0.97(2)	1.02(2)	0.90(2)	0.98(2)	0.96(2)	0.92(2)	0.87(2)
D Co	1.42(14)	1.76(18)	1.54(15)	1.35(14)	1.46(15)	1.59(16)	1.33(13)	1.13(12)
D Ni	7.24(73)	8.52(85)	5.39(55)	6.05(61)	7.46(75)	9.22(92)	6.13(63)	5.44(60)
D Mg	2.87(5)	3.46(5)	3.34(5)	2.52(5)	2.97(5)	2.89(5)	3.31(5)	2.54(5)
K _d (V-Mg)	0.085(10)	0.058(10)	0.066(10)	0.086(10)	0.072(10)	0.076(10)	0.066(10)	0.088(10)
K _d (Cr-Mg)	0.20(3)	0.18(2)	0.19(2)	0.23(3)	0.20(2)	0.20(2)	0.17(2)	0.22(3)
K _d (Mn-Mg)	0.26(3)	0.22(3)	0.25(3)	0.28(3)	0.24(3)	0.26(3)	0.21(2)	0.28(3)
K _d (Fe-Mg)	0.33(1)	0.28(1)	0.31(1)	0.36(1)	0.33(1)	0.33(1)	0.28(1)	0.35(1)
K _d (Co-Mg)	0.49(6)	0.51(5)	0.46(5)	0.53(6)	0.49(5)	0.55(6)	0.40(5)	0.44(5)
K _d (Ni-Mg)	2.52(26)	2.46(25)	1.61(17)	2.40(25)	2.51(26)	3.19(32)	1.85(20)	2.14(22)

719 **Table 4: Regression results for D(olivine/melt):** $D = a D(\text{Mg}) + b \text{NBO/T} + c \Delta\text{FMQ} + d (\text{S ppm}) + e$

Element	a	b	c	d	E	N	Std error	Studies
Ni	3.23(19)	-1.29(43)	-	-	-1.78(1.09)	82	1.00	2,3,4,5,6,7
Co	0.805(38)	-0.182(85)	-	-	-0.124(219)	69	0.20	2,3,4,5,7
Co (with S)	0.495(67)	-0.311(91)	-	-0.0000824 (253)	0.843(267)	117	0.23	1,2,3,4,5,7,8
Mn	0.206(6)	0.045(12)	-	-	0.0689(319)	121	0.054	2,3,4,9
V	-0.0619(123)	-0.0140(58)	-0.0398(29)	-	0.199(33)	116	0.051	2,7,9
Cr	-0.0448(578)	0.262(29)	-0.0404(139)	-	-0.0752(167)	113	0.252	2,4,9,10

720

721 1 – Gaetani and Grove, 1997; 2 – Tuff and O’Neill, 2010; 3 – LeRoux et al., 2011; 4 – Longhi et al., 2010; 5 – Herd et al., 2009; 6 –
 722 Filiberto et al., 2009; 7 – Elardo et al., 2011; 8 – this study; 9 – Mallmann and O’Neill, 2013; 10 – Hanson and Jones, 1998.